METHODS IN MOLECULAR BIOLOGY™

Series Editor
John M. Walker
School of Life Sciences
University of Hertfordshire
Hatfield, Hertfordshire, AL10 9AB, UK

For other titles published in this series, go to
www.springer.com/series/7651

Nitric Oxide

Methods and Protocols

Edited by

Helen O. McCarthy

School of Pharmacy, Queen's University Belfast, Northern Ireland, UK

Jonathan A. Coulter

School of Pharmacy, Queen's University Belfast, Northern Ireland, UK

Humana Press

Editors
Helen O. McCarthy
School of Pharmacy
Queen's University, Belfast
Northern Ireland BT9 7BL, UK
h.mccarthy@qub.ac.uk

Jonathan A. Coulter
School of Pharmacy
Queen's University, Belfast
Northern Ireland BT9 7BL, UK
j.coulter@qub.ac.uk

ISSN 1064-3745
ISBN 978-1-61737-963-5
DOI 10.1007/978-1-61737-964-2
e-ISSN 1940-6029
e-ISBN 978-1-61737-964-2
Springer New York Dordrecht Heidelberg London

Humana Press is part of Springer Science+Business Media (www.springer.com)

Preface

This book forms part of the highly acclaimed *Methods in Molecular Biology*™ series, which aims to provide a detailed reference manual giving a step-by-step approach to reproduce various complex protocols within your own laboratory. For each volume in this series, editors have included the most interesting and relevant methodologies published in the field in recent years, thereby providing access to the most novel experimental approaches. In addition, this series also provides a detailed notes section which documents specific information relating to particularly challenging aspects of a methodology.

The past two decades have seen an explosion in the number of research articles relating to both the physiological and pathological responses evoked by nitric oxide generation. Despite this, accurate quantification of nitric oxide in either in vitro or in vivo models remains challenging, due to the relatively unstable nature of the molecule.

This volume considers two of the main aspects of nitric oxide research. Section I of the book includes a review from an expert in tumor radiosensitization induced by various novel compounds, including nitric oxide. The review covers multiple facets of nitric oxide including its role in addiction, the cardiovascular system, the nervous system, and cancer. The remainder of Section I describes various disparate protocols relating to the direct detection and quantification of nitric oxide. These include techniques which detail how to image real-time in vivo generation of nitric oxide, quantify nitric oxide production in the rat brain, and detect ultralow levels of nitric oxide in the pM range.

Section II focuses primarily on techniques designed to either inhibit or enhance nitric oxide, with an aim to achieve therapeutic gain. These include inhibition of the nitric oxide synthase enzymes using viral, shRNA delivery systems to prevent cardiovascular dysfunction, peripheral neuropathy, and graft rejection. Other techniques highlighted deal with the overproduction of nitric oxide at target sites using novel nitric oxide releasing nanoparticles and biofilms.

We hope this book provides clarification on the numerous complex methodologies detailed in each chapter, proving to be an invaluable resource for anyone with an interest in nitric oxide research.

Helen O. McCarthy
Jonathan A. Coulter

Contents

Contributors

YONG CHOOL BOO • *Department of Molecular Medicine and Cell and Matrix Research Institute, BK21 Medical Education Program for Human Resources, Kyungpook National University School of Medicine, Daegu, Republic of Korea*

SUSANNE BURDAK-ROTHKAMM • *Stoke Mandeville Hospital, Histopathology Department, Aylesbury, UK*

CINZIA DI FRANCO • *CNR-IFN U.O.S. di BARI, Physics Department, University of Bari, Bari, Italy*

ANGELA ELIA • *CNR-IFN U.O.S. di BARI, Physics Department, University of Bari, I-0126 Bari, Italy*

JOEL M. FRIEDMAN • *Department of Physiology and Biophysics, Albert Einstein College of Medicine, Yeshiva University, Bronx, NY*

ADAM J. FRIEDMAN • *Division of Dermatology, Department of Physiology and Biophysics, Albert Einstein College of Medicine, Yeshiva University, Bronx, NY*

GEORGE HAN • *Department of Physiology and Biophysics, Albert Einstein College of Medicine, Yeshiva University, Bronx, NY*

JAMES HEWINSON • *Department of Physiology and Pharmacology, University of Bristol, Bristol, UK*

DAVID G. HIRST • *School of Pharmacy, Queen's University Belfast, Belfast, UK*

HAO HONG • *The State Key Laboratory of Pharmaceutical Biotechnology, School of Life Sciences, Nanjing University, Nanjing, People's Republic of China*

SEAN O. HYNES • *Regenerative Medicine Institute, National University of Ireland, Galway, Ireland*

HANJOONG JO • *Wallace H. Coulter Department of Biomedical Engineering at Georgia Tech, Emory University and Ewha Womans University, Atlanta, GA, USA*

SERGEY KASPAROV • *Department of Physiology and Pharmacology, University of Bristol, Bristol, UK*

CHI H. LEE • *School of Pharmacy, University of Missouri, Kansas City, MO, USA*

BEIHUI LIU • *Department of Physiology and Pharmacology, University of Bristol, Bristol, UK*

KEZHOU LIU • *Department of Biomedical Engineering, Zhejiang University, Hangzhou, People's Republic of China*

MARLENE LÚCIO • *REQUIMTE, Departamento de Química-Física, Faculdade de Farmácia, Universidade do Porto, Porto, Portugal*

PIETRO MARIO LUGARÀ • *CNR-IFN U.O.S. di BARI, Physics Department, University of Bari, Bari, Italy*

LUÍS M. MAGALHÃES • *REQUIMTE, Departamento de Química-Física, Faculdade de Farmácia, Universidade do Porto, Porto, Portugal*

CILLIAN MCCABE • *Regenerative Medicine Institute, National University of Ireland, Galway, Ireland*

FRANCISCO MONTERO • *Área de Fisiología, Facultad de Medicina, Universidad de Cádiz, Cádiz, Spain*

Bernardo Moreno-López • *Área de Fisiología, Facultad de Medicina, Universidad de Cádiz, Cádiz, Spain*
Gyeong In Mun • *Department of Molecular Medicine, Cell and Matrix Research Institute, BK21 Medical Education Program for Human Resources, Kyungpook National University School of Medicine, Daegu, Republic of Korea*
Enika Nagababu • *Molecular Dynamics Section, National Institute on Aging, National Institutes of Health, Baltimore, MD, USA*
Timothy O'Brien • *Regenerative Medicine Institute, National University of Ireland, Galway, Ireland*
Julian F.R. Paton • *Department of Physiology and Pharmacology, University of Bristol, Bristol, UK*
Barbora Piknova • *Molecular Medicine Branch, National Institute of Diabetes and Digestive and Kidney Diseases, National Institutes of Health, Bethesda, MD, UK*
Federico Portillo • *Área de Fisiología, Facultad de Medicina, Universidad de Cádiz, Cádiz, Spain*
Salette Reis • *REQUIMTE, Departamento de Química-Física, Faculdade de Farmácia, Universidade do Porto, Porto, Portugal*
Joana P.N. Ribeiro • *REQUIMTE, Departamento de Química-Física, Faculdade de Farmácia, Universidade do Porto, Porto, Portugal*
Joseph M. Rifkind • *Molecular Dynamics Section, National Institute on Aging, National Institutes of Health, Baltimore, MD, USA*
Tracy Robson • *School of Pharmacy, Queen's University Belfast, Belfast, UK*
Kai Rothkamm • *Health Protection Agency Centre for Radiation, Chemical & Environmental Hazards, Oxon, UK; Stoke Mandeville Hospital, Histopathology Department, Aylesbury, UK; Radiation Protection Division, Health Protection Agency, Chilton, Didcot, UK*
Alan N. Schechter • *Molecular Medicine Branch, National Institute of Diabetes, Digestive, Kidney Diseases, National Institutes of Health, Bethesda, MD, UK*
Marcela A. Segundo • *REQUIMTE, Departamento de Química-Física, Faculdade de Farmácia, Universidade do Porto, Porto, Portugal*
David N. Silverman • *Department of Pharmacology, University of Florida, Gainesville, FL*
Vincenzo Spagnolo • *CNR-IFN U.O.S. di BARI, Physics Department, University of Bari, Bari, Italy*
Carmen R. Sunico • *Área de Fisiología, Facultad de Medicina, Universidad de Cádiz, Cádiz, Spain*
Alexander A. Timoshin • *Institute of Experimental Cardiology, Russian Cardiology Research-and-Production Complex, Rosmedtechnology Corporation, Moscow, Russia*
Sarah L. Tressel • *Wallace H. Coulter Department of Biomedical Engineering at Georgia Tech, Emory University, Atlanta, GA, USA*
Chingkuang Tu • *Department of Pharmacology, University of Florida, Gainesville, FL*
Anatoly F. Vanin • *Semyonov Institute of Chemical Physics, Russian Academy of Sciences, Moscow, Russia*
Haibo Xu • *Department of Pharmacology, State Key Laboratory for Research and Development of Chinese Materia Medica, Chengdu University of Traditional Chinese Medicine, Chengdu, P.R. China*

YONG YANG • *Department of Biomedical Engineering, Hangzhou Dianzi University, Hangzhou, People's Republic of China*
JUNFENG ZHANG • *The State Key Laboratory of Pharmaceutical Biotechnology, School of Life Sciences, Nanjing University, Nanjing, People's Republic of China*
XIAOXIANG ZHENG • *Department of Biomedical Engineering, Zhejiang University, Hangzhou, People's Republic of China*

Chapter 10

Quantum Cascade Laser Technology for the Ultrasensitive Detection of Low-Level Nitric Oxide

Angela Elia, Pietro Mario Lugarà, Cinzia Di Franco, and Vincenzo Spagnolo

Abstract

Several spectroscopic methods based on mid-infrared quantum cascade lasers for the ultrasensitive detection of nitric oxide have been developed with detection limit in ppbv and sub-ppbv range. We will describe here a selection of the most effective techniques, i.e., laser absorption spectroscopy, cavity-enhanced spectroscopy, photoacoustic spectroscopy, and Faraday modulation spectroscopy. For each technique, advantages and drawbacks will be underlined.

Key words: Nitric oxide detection, quantum cascade lasers, absorption spectroscopy, cavity-enhanced spectroscopy, photoacoustic spectroscopy, Faraday modulation spectroscopy.

1. Introduction

The development of compact optical sensors for nitric oxide (NO) detection is of interest for different applications, such as environmental monitoring (1), vehicle exhaust control (2), industrial process control (3), and medical diagnostics (4).

Both optical and nonoptical analytical methods have been developed to measure ultralow concentrations of NO. Nonoptical approaches include mass spectrometry and gas chromatography. The main drawbacks of these techniques are size and cost of the apparatus, the need for sample conditioning, consumables, and the inability to make real-time and online measurements. The most advanced optical techniques are based upon either chemiluminescence or laser absorption processes. In particular, infrared

H.O. McCarthy, J.A. Coulter (eds.), *Nitric Oxide*, Methods in Molecular Biology 704,
DOI 10.1007/978-1-61737-964-2_10,

laser absorption spectroscopy (LAS) has become an extremely effective tool for the detection and quantification of molecular trace gases. The detection sensitivity of LAS ranges from ppmv (part per million in volume) down to pptv (part per trillion in volume) levels depending on the specific gas species and the detection method employed.

Several infrared spectroscopy techniques have been developed for NO monitoring in ppbv (part per billion in volume) and sub-ppbv range.

NO is a polar molecule and infrared (IR) active. The gas-phase NO molecule has two absorption bands near 5.2 and 2.6 μm. For highly sensitive spectroscopic trace detection, a suitable band must be selected. It should be characterized by strong absorption intensity, but isolated from other interfering species, i.e., water and carbon dioxide. In particular, the detection of NO is more effective in the mid-IR spectral region around 5.2 μm, where the strongest spectral feature has intensity lines of about $\sim 6.04 \times 10^{-20}$ cm/molecule and is separated from interference absorption bands.

Several types of laser sources are available in this spectral region. These include line-tunable carbon monoxide (CO) lasers, lead–salt diode lasers, quantum cascade lasers, and nonlinear laser sources such as optical parametric oscillators (OPO) and difference frequency generation (DFG) systems.

The ideal source for spectroscopic applications should have the following characteristics: (i) high optical power, to get high laser signal-to-noise ratios; (ii) narrow line width, to obtain good selectivity; (iii) single mode operation; (iv) low source noise and low amplitude fluctuations; (v) high stability to environmental conditions, i.e., temperature, pressure, humidity, and vibrations; (vi) high reliability; and (vii) compact and robust overall sensor package size.

The lead–salt lasers are difficult to incorporate into a commercial device because of their need for cryogenic cooling. Nonlinear generation of IR light via DFG or OPO (based on periodically poled lithium niobate crystals) provides a broad continuous tuning range (hundreds of cm^{-1}) (5–8). However, to reach the ppbv level of sensitivity with the low power achievable by DFG (up to few mW) (9–12), advanced detection schemes are needed. OPOs have relatively high power levels (1 W, continuous wave operation) and narrow line width (typically a few MHz over 1 s) and, therefore, represent an excellent source for sensitive spectroscopic gas analysis. In combination with fiber pump laser technology, the OPO-based sources offer the attractive advantage of a rather compact setup. However, to date, OPOs are less suitable for field applications as the cavity needs occasional tweaking. Until a few years ago, direct generation of tunable mid-IR radiation using solid-state lasers suffered especially from limited output

power, low-temperature operation, and limited tuning properties. Instead, quantum cascade lasers (QCLs) represent a valid choice, since they overcome some of the major drawbacks of other traditional mid-IR laser sources. These include the lack of continuous wavelength tunability, the large size and weight of gas lasers, low output power and cooling requirement of lead–salt diode lasers, and the complexity of nonlinear optical generators.

Several very effective approaches utilizing QCLs for the optical sensing of NO have been reported.

2. Properties of Quantum Cascade Lasers

Quantum cascade lasers have been constantly developed since their invention at Bell Laboratories in 1994 (13) and so far represent the most interesting source for optical sensors.

QCLs are unipolar semiconductor lasers based on inter-subband transitions in a multiple quantum-well heterostructure (*see* **Note 1**). Typical emission wavelengths can be varied in the range of 3–17 μm.

The innovations in QCLs led to the first demonstration of continuous wave (cw) operation at room temperature at the wavelength of 9 μm in 2002 (14). In 2003, Yu and colleagues (15) achieved room-temperature cw operation at shorter wavelengths and very large output powers by reducing the doping in the active region and ridge width. To achieve the single frequency required by chemical sensing applications, a Bragg grating was integrated into the laser waveguide for the first time at Bell Laboratories by Gmachl and coworkers, resulting in a distributed-feedback (DFB) laser operating at cryogenic temperatures (16).

The latest generation of QC-DFB lasers is based on a "top-grating" approach that takes advantage of the characteristics of a mid-IR waveguide. For mid-IR wavelengths below 15 μm, dielectric waveguides of low-doped semiconductor layers with a proper refractive index modulation are used (17). Furthermore, room-temperature commercial cw DFB-QCLs with an optical power larger than 100 mW (18, 19) and prototype lasers emitting up to few watts (20) have been developed.

QCLs generally require several amperes of current in cw operation, and compliance voltages of 5–10 V. The resulting thermal load to the laser is substantial, where good thermal management is necessary to reach room-temperature operation. In addition, the tuning range of a DFB-QCL covers one or two absorption lines of a gas. However, some applications are based on the detection of multicomponent gas matrix, requiring a large tuning range. Fortunately, the inter-subband transitions can be tailored to enable

the design of active regions with very large gain bandwidth. In 2004, Maulini and coworkers (21) demonstrated the first external cavity QCL (EC-QCL) operating in a cw over a record frequency span of 175/cm, using a bound-to-continuum QC structure with an optical power up to 10 mW. Coarse tuning can be obtained by rotating the grating, while changing the cavity length and laser chip temperature allows the fine tuning. The main advantage of EC-QCLs with respect to DFB-QCLs is a broader tuning range, limited only by the spectral bandwidth of its gain element. A broader tunability of several hundreds of wave numbers will allow the detection of entire absorption bands and enhance the flexibility of QCLs for trace gas analysis.

The usefulness of these lasers for spectroscopic applications has recently been demonstrated by Wysocki et al. (3) who used a thermoelectrically (TE) cooled cw EC-QCL for spectroscopic absorption measurement of NO (22).

3. Methods

3.1. Absorption Spectroscopy

Laser absorption spectroscopy (LAS) has a great potential for the detection and monitoring of trace gases. It operates on the principle that the amount of light absorbed by a gas is related to the concentration of the target species (*see* **Note 2**).

For each gas a strong absorption line, preferably free of interference due to other gases in the sample cell, must be selected. The strongest molecular rotational–vibrational transitions, which are desired to perform ultrasensitive concentration measurement, are in the mid-IR spectral region (*see* **Note 3**).

The most important advantage of LAS is the ability to provide absolute quantitative assessments of species. Its biggest disadvantage relies on the measurement of a small change in a high level optical power; any noise introduced by the light source or the transmission through the optical system will decrease the sensitivity of the technique. Laser absorption spectrometric techniques are therefore often limited to detection of absorbance $\sim 10^{-3}$, which is far away from the theoretical shot noise level, which for a single-pass technique is in the 10^{-7}–10^{-8} range. This sensitivity is insufficient for many types of applications.

Obtaining detection sensitivities at ppbv or sub-ppbv levels requires either long effective optical path lengths or suppression of laser and optical noise. Long optical path lengths are typically obtained in multipass absorption cells.

There are three types of multipass cells in use (23–26): White cells (*see* **Note 4**), Herriott cells (*see* **Note 5**), and astigmatic mirror cells (*see* **Note 6**).

The designs of the three types of cells must fulfill specific rules so that the beam goes out of the cell after a controlled number of passes, especially in the case of astigmatic cells. Optical output of the cell decreases exponentially with the number of passes. In order to have small absorptions and maximum sensitivity, the optimal number of reflections corresponds to the output light being $1/e$ times the input light. However, as long as the noise is determined by laser intensity fluctuations, rather than by detector noise, additional passes will improve the signal-to-noise ratio (SNR).

In 2006, Moeskops and coworkers (27) monitored the unresolved NO doublet at 1,850.18/cm with a detection limit of 0.2 ppbv corresponding to a minimal detectable absorption of 8.8×10^{-9}/cm $Hz^{1/2}$ (*see* **Note 7**).

Atmospheric NO was detected by MacManus and coworkers (28) via a totally noncryogenic spectrometer with a detection limit of 0.1 ppbv in pulsed mode and 0.03 ppbv in cw after an average time of 30 s (*see* **Note 8**).

The use of a single-pass cell resulted in an absorption spectrometer less sensitive, as reported by Kasyutich and coworkers (29). They reported a minimum detection limit of 2.7 ppmv in plasma diagnostics (*see* **Note 9**).

3.2. Cavity-Enhanced Spectroscopy

Cavity-enhanced spectroscopy (CES) methods provide a much higher sensitivity than conventional long optical path length absorption spectroscopy (*see* **Note 10**).

Different techniques have been implemented. In particular, cavity ring-down spectroscopy (CRDS) is the most popular CES embodiment. It is a direct absorption technique which can be performed with pulsed or continuous light sources. It is based on the measurement of the decay time of an injected laser beam in a high-finesse optical cavity in the presence of an absorbing gas by measuring the time dependence of the light leaking out of the cavity (*see* **Note 11**).

The technique based on cw laser sources was first proposed by Romanini et al. (30) using cw near-IR DFB diode lasers and was extended to QCL sources by Paldus et al. (31).

CRDS with cw QC-DFB laser has been successfully applied to the detection of NO at ppbv concentrations by Kosterev et al. (*see* **Note 12**) (32). The schematic NO sensor is shown in **Fig. 10.1** (*see* **Note 13**). The authors demonstrated the detection of NO in pure N_2 with concentrations at ppbv levels with a 0.7-ppbv standard error for a data collection time of 8 s and with 4,000 ring-down events. It was not possible to use this sensor directly for measurements of NO concentration in exhaled air (10 ppbv) because of a strong interference with CO.

Another technique based on a high-finesse optical cavity is called "integrated cavity output spectroscopy" (ICOS) or

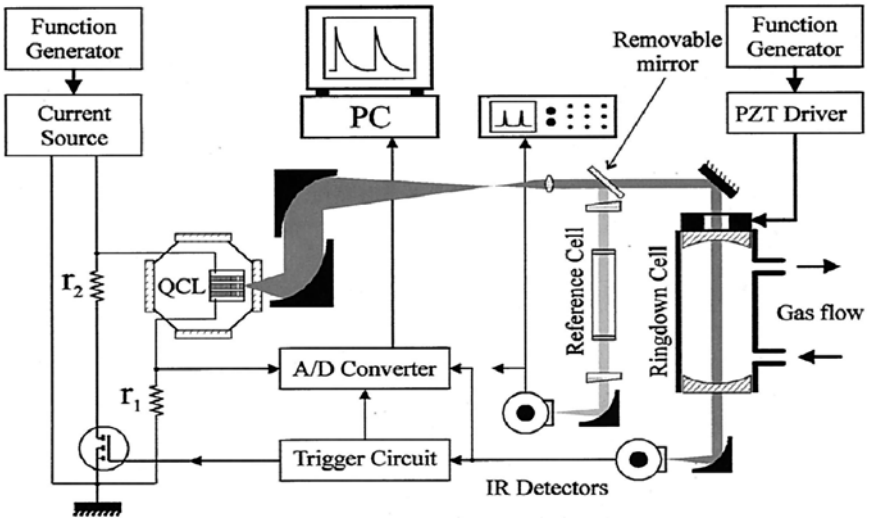

Fig. 10.1. Schematic of a CRDS-based gas sensor. r_1: current monitor resistor; r_2: current-limiting resistor. Two wedged ZnSe windows shown near the reference cell were used to form an etalon for fine frequency calibration. (Reproduced from ref. (32) with kind permission of The Optical Society of America.)

"cavity-enhanced absorption spectroscopy" (CEAS). Laser light is coupled into the high-finesse cavity via accidental coincidences of the laser frequencies and the cavity eigenmodes. The alignment of the cavity mirrors and the laser beam are optimized in order to maximize the number of transverse modes excited. Intensity radiation leaking out of the optical cavity is time-integrated and averaged over many cavity modes. Subsequently, the intensity radiation is inversely proportional to the total cavity losses which can be used to determine the absorption of the intracavity medium (*see* **Note 14**).

This approach was demonstrated with a cw QC-DFB laser in 2001 (33) for the detection of NO in human breath for biomedical applications (*see* **Note 15**). The detection limit was found to be 16 ppbv and was limited by a baseline noise of 1% (averaging 10 QC laser scans) which is intrinsic to this technique and results from the mode structure of the cavity transmission spectrum due to the incomplete averaging of cavity modes.

Some improvements in the baseline noise can be achieved with a recently developed off-axis ICOS (OA-ICOS). In this configuration, the laser beam is directed off-axis with respect to the cavity axis in order to increase the spectral density of cavity modes and thus minimize the noise in the absorption spectra by improving the averaging of the cavity output.

The off-axis ICOS measurement technique requires a less critical alignment of the exciting laser beam and is more insensitive to vibrations and misalignments than CRDS and on-axis ICOS.

Several QCL-based off-axis ICOS systems for the detection of NO have been reported with sensitivities in the ppbv level (34–38).

The first NO analyzer based on an off-axis ICOS and cw liquid-N_2-cooled QCL was developed in 2004 to measure NO concentrations in exhaled human breath (34). In combination with a wavelength modulation technique, a noise-equivalent (SNR = 1) sensitivity of 2 ppbv in a nasal breath sample was demonstrated for a 15 s data acquisition and integration time.

Two years later, an off-axis ICOS sensor (36, 37) based on a thermoelectrically cooled DFB-QCL operating in cw mode at 5.45 μm combined with a wavelength modulation technique was developed to measure NO concentrations at the sub-ppbv levels. A schematic of the sensor is reported in **Fig. 10.2**. A noise-equivalent minimum detection limit of 0.7 ppbv with a 1 s observation time was achieved (36) in N_2 and 1.2 ppbv with a 4 s observation time in exhaled breath samples (37).

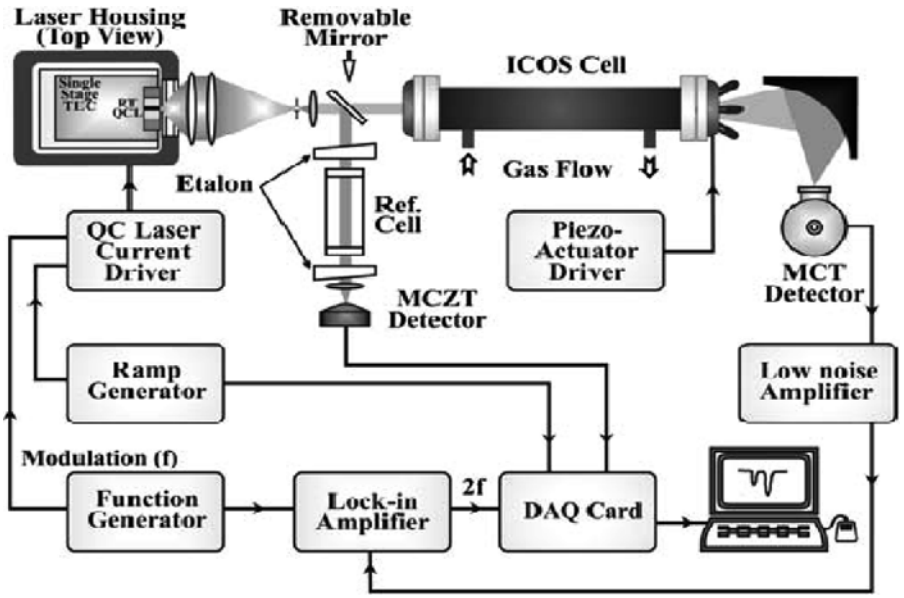

Fig. 10.2. TEC-cw-DFB-QCL-based OA-ICOS sensor. MCT is a cryogenically cooled photovoltaic HgCdTe detector and MCZT is a thermoelectrically cooled HgCdZnTe photodetector. (Reproduced from ref. 36 with kind permission of Springer Science and Business Media.)

More recently, McCurdy et al. (38) have reported an off-axis ICOS sensor capable of real-time detection of NO and CO_2 in a single breath cycle, achieving a NO detection limit of 0.4 ppbv with a 1 s integration time, in good agreement with the data acquired with a commercial chemiluminescence NO gas analyzer.

3.3. Photoacoustic Spectroscopy

Photoacoustic spectroscopy (PAS) represents an effective method for sensitive trace gas detection. PAS is an indirect technique in

which the effect on the absorbing medium and not the direct light attenuation is detected. In particular, it is based on the generation of an acoustic wave resulting from the absorption of modulated light of appropriate wavelength by molecules. The amplitude of this sound wave is directly proportional to the gas concentration and can be detected with a sensitive microphone if the laser beam is modulated in the audio frequency range (*see* **Note 16**).

In combination with QCLs, PAS offers the advantage of high sensitivity (ppbv detection limits), large dynamic range, compact setup, fast time-response, and simple optical alignment, if compared with other competing detection schemes, such as multipass absorption spectroscopy or cavity ring-down spectroscopy, which offer similar performances but require more sophisticated equipments.

PAS with DFB-QC laser for the detection of NO has been successfully demonstrated in 2005 by Elia et al. (39); a detection limit of 500 ppbv has been reported. The photoacoustic sensor for the detection of NO consisted of a commercially available distributed feedback quantum cascade laser source, a resonant photoacoustic cell, and a signal acquisition and processing equipment (*see* **Note 17**). In **Fig. 10.3**, a schematic diagram of the optoacoustic sensor is reported.

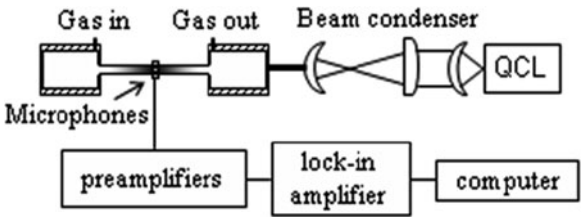

Fig. 10.3. Schematic diagram of the optoacoustic sensor.

More recently, the same group obtained a detection limit of 150 ppbv with a 10 s integration time constant for the detection of NO (40). This improved result is mostly due to improvements in the PA cell and damping of electromagnetic noise sources.

The Groupe de Spectrometrie Moleculaire et Atmospherique (Reims, France) developed a Helmholtz resonant photoacoustic sensor for NO detection (*see* **Note 18**). An extrapolated detection limit of 20 ppb of NO in nitrogen with a laser power of 3 mW was demonstrated (41). The presence in this region of interferences from water vapor lines prevents NO detection in air with a detection limit lower than 1 ppmv. More recently Spagnolo et al. (42) demonstrated a NO sensor based on quartz-enhanced photoacoustic (QEPAS) detection and an external cavity (EC) quantum cascade laser. The key innovation of QEPAS is to detect optically generated sound using a sharply resonant piezoelectric quartz tuning fork transducer. The NO concentration resulting in

a noise-equivalent signal was found to be 15 ppbv, with 100-mW optical excitation power and a data acquisition time of 5 s.

3.4. Faraday Spectroscopy

Faraday modulation spectroscopy (FMS) is an alternative detection technique capable of enhancing the sensitivity of LAS for radicals and ions (43–45). The absorption lines of radicals can be tuned by an external magnetic field that breaks the magnetic degeneracy of the rotational states (Zeeman effect). The resulting frequency shift of transitions is different for left-handed and right-handed circularly polarized light, giving rise to different refractive indices for these polarization components at a given radiation wavelength (circular birefringence). As a light beam, originally linearly polarized, propagates through the sample, this anisotropy leads to a rotation of the polarization axis. This magnetically induced birefringence in a longitudinal field and the related rotation of the polarization axis of linearly polarized light is called Faraday effect. The rotation is detected by means of putting the sample between nearly crossed polarizers. In this way, laser amplitude noise is largely suppressed. Also, employing a static magnetic field $B > 0$ in combination with a tunable laser, the sensitivity of direct absorption spectroscopy can be improved by 2–3 orders of magnitude. Since NO is the only radical in ambient air with a spectrum near $\lambda = 5.2$ μm, this spectroscopic approach coupled with QCLs is advantageous since there is no interference from other constituents in the air sample. Also, this technique enables the detection of NO at low ppbv concentration levels that are typical for biomedical applications. Thus, FMS combined with polarization detection is one of the most sensitive spectroscopic methods in the mid-IR wavelength range.

The typical experimental setup of FMS employing QCLs is shown in **Fig. 10.4** (43). The QCL source emits in the wavelength region around 5.2 μm. The laser beam passes through a Rochon polarizer and is then fed through a detection cell which is inside a copper wire coil for the application of a magnetic field. A second Rochon polarizer behind the cell is set to the crossed position with a slight offset angle. The transmitted portion is focused by means of a parabolic mirror to a liquid-N_2-cooled indium-antimonide (InSb) photodetector. If the QCL frequency is in resonance with a NO transition, and a magnetic field is applied, the polarization axis of the laser beam is slightly rotated due to the Faraday effect. Thus, a corresponding part of the light passes through the analyzer and reaches the detector (*see* **Note 19**). The obtained signal is proportional to the NO concentration inside the cell. Since a continuously tunable QCL is used, a servo loop is needed to stabilize the laser frequency to the NO absorption frequency. The setup of the frequency stabilization is also shown in **Fig. 10.4**.

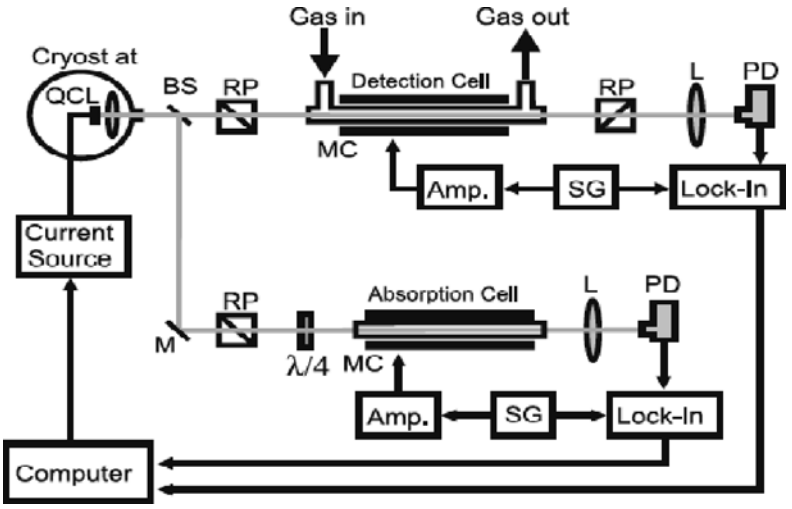

Fig. 10.4. Schematic of the Faraday modulation spectrometer. Both the spectrometer and the laser frequency stabilization utilize the fact that NO is a radical and, thus, transition frequencies are tunable with a magnetic field. For sensitive detection (*upper part*), the Faraday rotation of the polarization axis is utilized. For the frequency stabilization (*lower part*), the Zeeman detuning of the transition frequency is exploited. RP: Rochon polarizer; MC: magnetic coil; SG: sinus generator; PD: photodetector; M: mirror; BS: beam splitter; L: lens. (Reproduced from ref. 43 with kind permission of Springer Science+Business Media.)

A $\lambda/4$-plate transforms the linear polarization into a circular one. The circular polarized laser light passes through a cell filled with pure NO at a pressure <1 mbar and is focused onto a liquid-N_2-cooled InSb photodetector. Again, there is a modulation coil around the cell in order to use the Zeeman effect to tune the absorption frequency. The sinusoidal modulation of the absorption and its detection by a lock-in amplifier result in a signal shape similar to the first derivative of the absorption line, showing a zero-crossing at the line center. This error signal is fed back to the QC laser current for frequency stabilization.

The detection limit, i.e., the noise-equivalent sensitivity of the spectrometer, was determined by monitoring different dilutions of a certified gas mixture in air, typically NO in nitrogen. The linearity of signal and NO concentration has been checked over by one order of magnitude and the noise-equivalent NO concentration was 25 ppbv (in air), using an averaging time of 300 ms. This time resolution is required, for example, for medical breath analysis. When the averaging time is increased to 10 s, the detection limit achieved is 4 ppbv NO (in air), suitable for monitoring the NO release from liquids.

Faraday modulation spectroscopy has also been employed for the simultaneous detection of ^{14}NO and ^{15}NO by using a cw distributed feedback QCL operating near 5.4 μm. The simultaneous detection was performed using a fast laser frequency switching between the two isotopologues with a time resolution of 2 s. The isotope ratio has been determined with a precision (1σ) of 0.052% at 800 s averaging time for 100 ppmv NO gas (44).

Very recently, a transportable prototype Faraday rotation spectroscopic system based on a tunable external cavity QCL has been developed. A broadly tunable laser source allows targeting the optimum $Q_{3/2}(3/2)$ molecular transition at 1,875.81/cm of the NO fundamental band. For an active optical path of 44 cm and 1 s lock-in time constant, a minimum NO detection limit (1σ) of 0.38 ppbv is obtained using a liquid-N_2-cooled InSb photodetector (45).

3.5. Comparison Between Different Methods

In **Table 10.1**, a detailed comparison between different spectroscopic techniques in terms of advantages and drawbacks is reported.

Direct laser absorption techniques give the lowest detection limit (pptv) thanks to long effective optical path lengths and absolute quantitative assessments of species. However, this sensitivity can only be reached with complex and bulky apparatus such as multipass cell and cryogenically cooled low-noise detectors. To obtain longer optical paths (up to several kilometers) high-finesse optical cavity (such as for CRDS and ICOS) can be employed. However, cavity-enhanced approaches present disadvantages for practical applications mostly in terms of setup compactness, robustness, and sensitivity to optical alignment, and thus do not represent the best solution for in situ and online NO detections.

An alternative solution may be photoacoustic spectroscopy. This method has the advantages of low sensitivity to optical alignment, ease of use, portability, and high dynamic range. Also, methods based on the Faraday effect have demonstrated good sensitivity; however, they can be employed only for paramagnetic molecules and thus not in multidetection systems.

Finally, the best results obtained for the reported spectroscopic techniques are summarized in **Table 10.2**.

4. Notes

1. QCLs are designed by means of band-structure engineering and grown by molecular beam epitaxy techniques (13). The benefit of this approach is a widely variable transition energy primarily regulated by the thicknesses of the quantum well and barrier layers of the active region rather than the band gap as in diode lasers.
2. Light of known intensity is directed through a gas sample cell and the amount of light transmitted through the sample cell is measured by a detector. If we assume incident

Table 10.1
Advantages and drawbacks of QCL-based spectroscopic techniques

Techniques	LAS	CRDS	OA-ICOS	PAS	FMS
Detection limit	ppbv or sub-ppbv	ppbv	ppbv	Tens of ppbv	ppbv
Advantages	Sub-ppbv detection limit thanks to long effective optical path lengths; absolute quantitative assessments of species	Extremely long effective path length with small cells; intrinsic insensitivity to light source intensity fluctuations	Extremely long effective path length with small cells; less critical alignment of the exciting laser beam than CRDS	Low sensitivity to optical alignment; ease of use and high dynamic range; simple optical alignment	No need for multipass- or high-finesse cavities for detection limit enhancement; no interference from other constituents in the air sample
Drawbacks	Complex apparatus; bulky multipass cells	Liquid-nitrogen-cooled detector or lasers; sensitivity of the apparatus to optical alignment	Liquid-nitrogen-cooled detector or lasers	Sensitivity to external acoustic noise	Can be employed only for paramagnetic molecules

Table 10.2
Best results achieved with QCL-based sensors

References	Method	λ (μm)	QCL	Detector cooling	Detection limit (ppbv)	Recording time (s)
28	QCLAS	5.3	cw near RT	TE	0.03	30
32	CRDS	5.2	cw cryogenic	Cryogenic	0.7	8
35	OA-ICOS	5.2	cw cryogenic	Cryogenic	0.4	1
40	PAS	5.3	Pulsed RT	–	150	10
42	QEPAS	5.3	EC, cw TE	–	15	5
45	FMS	5.3	cw TE	Cryogenic	0.38	1

light intensity, $I_0(x = 0, \lambda)$, and transmitted light intensity, $I(x, \lambda)$, the Lambert–Beer's law relates the transmitted light to the incident light and the absorption coefficient of the sample, $\alpha(\lambda)$, as $I(x, \lambda) = I_0 \cdot \exp[-\alpha(\lambda)x]$, where λ is the wavelength and x is the path length. Concentration is determined from the absorption coefficient.

3. The usefulness of laser spectroscopy in the MIR region is limited by the properties of available IR laser sources, i.e., lead–salt diode lasers, coherent sources based on difference frequency generation, optical parametric oscillators, tunable solid-state lasers, and quantum and interband cascade lasers. In most cases these sources work only at cryogenic temperature or in pulsed mode.
4. The White cell (23, 24) is the oldest arrangement. It consists of two semicircular mirrors, called the "D" mirrors, closely spaced along a common diameter facing a third mirror with two notches in a nearly confocal arrangement. The probe beam enters through one notch and emerges through the other. The number of passes is varied by changing the "D" mirror angle.
5. The Herriott cell (25) has two identical spherical mirrors separated by almost their diameter of curvature (nearly concentric) facing each other. A probe beam launched through a hole in one of the mirrors at an angle to the optical axis completes several number of passes between the mirrors and exits through the same hole (or a hole in the other mirror). The beam bounce pattern and path length are controlled by adjusting the mirror separation.
6. Astigmatic mirror cells (26) are variations of the Herriott cell that spread the light spots over the entire mirror surfaces. This greatly increases the number of spots achievable without overlapping spots and therefore the number

of passes. This cell type is also more compact and possesses the smallest cell volume to effective path length ratio. In such a multipass cell, the number of passes is typically configured for 90–238, which results in effective optical path lengths from 18 to 210 m for mirror separations of 0.3–0.9 m, thus providing a rising improvement in signal strength.

7. Moeskops et al. (27) used a thermoelectrically cooled cw QCL operating in the wavelength range from 1,854 to 1,874/cm. The collimated radiation was directed into a multipass optical cell (Aerodyne, AMAC-76) with an absorption path length of 76 m and a volume of 300 mL at a pressure of 100 mbars.
8. The NO sensor developed by McManus et al. (28) consists of a cw QCL operating near room temperature at 1,900.07/cm (5.3 μm), a 69-m astigmatic multipass cell, and a TE-cooled IR detector. The pattern of reflections on the astigmatic cell mirrors has been designed to minimize optical interference fringes, which were substantially greater with cw mode than with pulsed operation.
9. Kasyutich et al. (29) integrated in the spectrometer a 1,900/cm cw QCL as source and a thermoelectrically cooled HgCdZnTe photovoltaic detector. The reported results were demonstrated for a 100 averaged spectra acquired within 1.25 s and a single-pass cell of 21 cm base length at about 100 Torr.
10. Cavity-enhanced absorption spectroscopy requires high excitation power (>1 mW) because of reduced transmission through a high-finesse optical cavity and a very sensitive detector (usually cryogenically cooled) characterized by low noise. Considering that the QCLs optical power has been steadily improved in the past few years and now commercial sources with optical power up to 1 W and prototype laser emitting up to few watts are available, the detection sensitivities of these techniques will largely improve allowing use of less sensitive but thermoelectrically cooled detectors, which are more suitable for the development of portable gas sensors.
11. CRDS has a significantly higher sensitivity than conventional absorption spectroscopy thanks to the large effective path lengths (several kilometers) that can be realized in a high-finesse optical cavity (with reflectivities of $R >$ 99.99%) with a small sample volume, and the intrinsic insensitivity to light source intensity fluctuations.
12. The laser frequency is slowly scanned across the selected absorption line of NO and one of the cavity mirrors is dithered back and forth to ensure periodic, random

coincidences of the laser frequency with a cavity mode. When the resonance occurs and the cavity is filled with the gas sample, the laser beam is abruptly interrupted or set off-resonance, and the relaxation time of the light leaking out of the cavity is measured.

The ringdown time for a two-mirror cavity with the same reflectivity $R \approx 1$ is defined by:

$$\tau = \frac{l}{c} \frac{1}{\alpha l + (1 - R)}$$

where l is the cavity length, c is the speed of light, R is the reflectivity of the cavity mirrors, and α is the absorption coefficient of the sample filling the cavity. Thus, the absorption coefficient can be determined by measuring the decay rate by the following equation:

$$\alpha = \frac{1}{c} \left(\frac{1}{\tau} - \frac{1}{\tau_{\text{empty}}} \right)$$

where τ_{empty} is the decay constant of the cavity in the presence of a nonabsorbing sample.

13. The 37-cm-long high-finesse optical cavity was formed by two concave mirrors with a 6 m radius of curvature. A cw liquid-nitrogen-cooled DFB-QCL operating at 5.2 μm was used as a tunable single-frequency light source to access the unresolved $R(13.5)$ components of the fundamental absorption band of NO located at 1,921.599 and 1,921.601/cm. The laser current was manipulated both for laser frequency tuning and abrupt interruptions of the laser radiation. A liquid-N_2-cooled photovoltaic HgCdTe detector was used to monitor the radiation.

14. The transmission of the cavity in the case of perfect spatial coupling is given by:

$$I = I_0 \frac{(1 - R)^2}{2\,[(1 - R) + \alpha L]}$$

where I_0 is the initial laser power, α is the absorption coefficient, R is the reflectivity of the mirrors, and L is the cavity length.

In the case of weak absorption ($\alpha L << 1 - R$), the previous equation becomes:

$$\frac{I}{I_0} \approx \frac{1 - R}{2} \left(1 - \frac{\alpha L}{1 - R} \right)$$

where $\frac{L}{1-R}\alpha$ is the effective path lengths.

15. The laser source is operated near 5.2 μm with a maximum output power of 80 mW. The 35.5-cm-long high-finesse cavity consists of two dielectric mirrors ($R = 99.995\%$ at 5.2 μm, radius of curvature of 6 m) and is characterized by an effective path length of $L = 670$ m.
16. The PA signal measured by the microphone is given by:

$$S = C \cdot P(\lambda) \cdot \alpha(\lambda)$$

where C is the cell constant in the unit of Vcm/W, P the optical power of the laser source, and α the absorption coefficient which is related to the gas concentration (N, number density of molecules) and absorption cross section (σ) by $\alpha = N\sigma$.

The cell constant depends on the geometry of the sample cell, the beam profile, the microphone response, and the nature of the acoustic mode. Thus, the sensitivity of a PA sensor can be considerably improved by using resonant photoacoustic sample cells and modulating the laser radiation at a frequency equivalent to an acoustic mode of the cell. As the equation implies, the recorded PA signal can be enhanced also using high-power laser sources emitting in the fundamental absorption region.

17. The laser operated at room temperature in pulsed mode (pulse duration of 42 ns and a duty cycle of 1.4%) with an optical average power of 4 mW at a wavelength around 5.3 μm. The resonant PA cell was a cylindrical stainless-steel resonator of 120 mm length and 4 mm radius with $\lambda/4$ buffer volumes on each side used as acoustic filters. The resonator, designed to be exited in the first longitudinal mode at 1,380 Hz, was equipped with four electret microphones (Knowles EK 3024, 20 mV/Pa), placed at the position of maximum acoustic amplitude to increase the signal-to-noise ratio.
18. The sensor is based on a differential Helmholtz resonant cell formed by two stainless-steel cylindrical volumes (10 cm in length, 5 mm radius) linked by two capillaries (10 cm in length, 2 mm radius) and characterized by a resonance frequency of 315 Hz. The differential measurement, obtained by measuring the PA signal with two microphones (one in each volume), eliminates a great part of the acoustic noise and raises the acoustic signal by a factor of 2. The cell was coupled with a cw DFB-QC laser working at cryogenic temperature in cw mode in the 5.4 μm region.
19. The magnetic field is sinusoidally modulated (with modulation frequency of few kHz). A typical value for the applied alternating magnetic field B is 1×10^{-2} Tesla (RMS),

which results in a periodic Zeeman shift in the order of ±100 MHz. For demodulation of the signal, a lock-in amplifier is used. Assuming that the polarizers are slightly uncrossed, the output of the lock-in amplifier is proportional to the signal amplitude. The demodulated signal is recorded by a personal computer and the results may be displayed in real time.

Acknowledgements

We acknowledge partial financial support from Regione Puglia – Project DM01 related with the Apulian Technological District on Mechatronics-MEDIS.

References

1. Nelson, D. D., Shorter, J. H., McManus, J. B., and Zahniser, M. S. (2002) Sub-part-per-billion detection of nitric oxide in air using a thermoelectrically cooled mid-infrared quantum cascade laser spectrometer. *Appl Phys B* 75, 343–350.
2. Weber, W. H., Remillard, T. J., Chase, R. E., Richert, J. F., Capasso, F., Gmachl, C., Hutchinson, A. L., Sivco, D. L., Baillargeon, J. N., and Cho, A. Y. (2002) Using a wavelength-modulation quantum cascade laser to measure NO concentration in the parts-per-billion range for vehicle emissions certification. *Appl Spectrosc* 56, 706–714.
3. Wysocki, G., Kosterev, A. A., and Tittel, F. K. (2005) Spectroscopic trace-gas sensor with rapidly scanned wavelengths of a pulsed quantum cascade laser for in situ NO monitoring of industrial exhaust systems. *Appl Phys B* 80, 617–625.
4. Kharitonov, S. A. and Barnes, P. J. (2000) Clinical aspects of exhaled nitric oxide. *Eur Respir J* 16, 781–792.
5. van Herpen, M. M. J. W., Bisson, S. E., Ngai, A. K. Y., and Harren, F. J. M. (2004) Combined wide pump tuning and high power of a continuous-wave, singly resonant optical parametric oscillator. *Appl Phys B* 78, 281–286.
6. Bisson, S. E., Armstrong, K. M., Kulp, T. J., and Hartings, M. (2001) Broadly tunable, mode-hop-tuned cw optical parametric oscillator based on periodically poled lithium niobate. *Appl Opt* 40, 6049–6055.
7. Müller, F., Popp, A., Kühnemann, F., and Schiller, S. (2003) Transportable, highly sensitive photoacoustic spectrometer based on a continuous-wave dual cavity optical parametric oscillator. *Opt Express* 11, 2820–2825.
8. Klein, M. E., Laue, C. K., Lee, D. H., Boller, K. J., and Wallenstein, R. (2000) Diode-pumped singly resonant continuous-wave optical parametric oscillator with wide continuous tuning of the near-infrared idler wave. *Opt Lett* 25, 490–492.
9. Tittel, F. K., Richter, D., Fried, A. (2003) Mid-infrared laser applications in spectroscopy, In (Sorokina, I. T., Vodopyanov, K. L. eds.), *Solid-State Mid-Infrared Laser Sources*. Springer, Berlin. pp. 445–516.
10. Bisson, S. E., Kulp, T. J., Levi, O., Harris, J. S., and Fejer, M. M. (2006) Long-wave IR chemical sensing based on difference frequency generation in orientation-patterned GaAs. *Appl Phys B* 8, 199–206.
10. Chen, W. D., Poullet, E., Burie, J., Boucher, D., Sigrist, M. W., Zondy, J. J., Isaenko, L., Yelisseyev, A., and Lobanov, S.. Widely tunable continuous-wave mid-infrared radiation (5.5–11 μm) by difference-frequency generation in $LiInS_2$ crystal. *Appl Opt* 44, 4123–4129.
12. Richter, D. and Weibring, P. (2006) Ultra-high precision mid-IR spectrometer I: design

and analysis of an optical fiber pumped difference-frequency generation source. *Appl Phys B* 82, 479–486.
13. Faist, J., Capasso, F., Sivco, D. L., Sirtori, C., Hutchinson, A. L., and Cho, A. Y. (1994) Quantum cascade laser. *Science* 264, 553–556.
14. Beck, M., Hofstetter, D., Aellen, T., Faist, J., Oesterle, U., Ilegems, M., Gini, E., and Melchior, H. (2002) Continuous wave operation of a mid-infrared semiconductor laser at room temperature. *Science* 295, 301–305.
15. Yu, J. S., Slivken, S., Evans, A., Doris, L., and Razeghi, M. (2003) High-power continuous-wave operation of a 6 μm quantum-cascade laser at room temperature. *Appl Phys Lett* 83, 2503–2505.
16. Gmachl, C., Faist, J., Baillargeon, J. N., Capasso, F., Sirtori, C., Sivco, D. L., and Cho, A. Y. (1997) Complex-coupled quantum cascade distributed-feedback laser. *Photon Technol Lett* 9, 1090–1092.
17. Kohler, R., Gmachl, C., Tredicucci, A., Capasso, F., Sivco, D. L., Chu, S. N. G., and Cho, A. Y. (2000) Single-mode tunable, pulsed, and continuous wave quantum-cascade distributed feedback lasers at 4.6–4.7 μm. *Appl Phys Lett* 76, 1092–1094.
18. DFB CW Room-Temperature Lasers. Available online: http://www.alpeslasers.ch, Jul 2009.
19. Tunable Mid-IR External Cavity Lasers. Available online: http://www.daylightsolutions.com, Jul 2009.
20. Yu, J. S., Slivken, S., Evans, A., Darvish, S. R., Nguyen, J., and Razeghi, M. (2006) High-power ~ 9.5 μm quantum-cascade lasers operating above room temperature in continuous-wave mode. *Appl Phys Lett* 88, 091113–091115.
21. Maulini, R., Beck, M., Faist, J., and Gini, E. (2004) Broadband tuning of external cavity bound-to-continuum quantum-cascade lasers. *Appl Phys Lett* 84, 1659–1661.
22. Wysocki, G., Curl, R. F., Tittel, F. K., Maulini, R., Bulliard, J. M., and Faist, J. (2005) Widely tunable mode-hop free external cavity quantum cascade laser for high resolution spectroscopic applications. *Appl Phys B* 81, 769–777.
23. White, J. U. (1942) Long optical paths of large aperture. *J Opt Soc Am* 32, 285–288.
24. Pilston, R. G. and White, J. U. (1954) A long path gas absorption cell. *J Opt Soc Am* 44, 572–573.
25. Herriott, D., Kogelnik, H., and Kompfner, R. (1964) Off-axis paths in spherical mirror interferometers. *Appl Opt* 3, 523–526.
26. McManus, J. B., Kebabian, P. L., and Zahniser, M. S. (1995) Astigmatic mirror multipass absorption cells for long-path length spectroscopy. *Appl Opt* 34, 3336–3348.
27. Moeskops, B. W. M., Critescu, S. M., and Harren, F. J. M. (2006) Sub-part-per-billion monitoring of nitric oxide by use of wavelength modulation spectroscopy in combination with a thermoelectrically cooled, continuous-wave quantum cascade laser. *Opt Lett* 31, 823–825.
28. McManus, J. B., Nelson, D. D., Herndon, S. C., Shorter, J. H., Zahniser, M. S., Blaser, S., Hvozdara, L., Muller, A., Giovannini, M., and Faist, J. (2006) Comparison of cw and pulsed operation with a TE-cooled quantum cascade infrared laser for detection of nitric oxide at 1900 cm^{-1}. *Appl Phys B* 85, 235–241.
29. Kasyutich, V. L., Holdsworth, R. J., and Martin, P. A. (2008) Mid-infrared laser absorption spectrometers based upon all-diode laser difference frequency generation and a room temperature quantum cascade laser for the detection of CO, N_2O and NO. *Appl Phys B* 92, 271–279.
30. Romanini, D., Kachanov, A. A., Sadeghi, N., and Stoeckel, F. (1997) CW cavity ring down spectroscopy. *Chem Phys Lett* 264, 316–322.
31. Paldus, B. A., Harb, C. C., Spence, T. G., Zare, R. N., Gmachl, C., Capasso, F., Sivco, D. L., Baillargeon, J. N., Hutchinson, A. L., and Cho, A. Y. (2000) Cavity ringdown spectroscopy using mid-infrared quantum-cascade lasers. *Opt Lett* 25, 666–668.
32. Kosterev, A., Malinovsky, A. L., Tittel, F. K., Gmachl, C., Capasso, F., Sivco, D. L., Baillargeon, J. N., Hutchinson, A. L., and Cho, A. Y. (2001) Cavity ringdown spectroscopic detection of nitric oxide with continuous-wave quantum-cascade laser. *Appl Opt* 40, 5522–5529.
33. Menzel, L., Kosterev, A. A., Curl, R. F., Tittel, F. K., Gmachl, C., Capasso, F., Sivco, D. L., Baillargeon, J. N., Hutchinson, A. L., Cho, A. Y. et al. (2001) Spectroscopic detection of biological NO with a quantum cascade laser. *Appl Phys B* 72, 859–863.
34. Bakhirkin, Y. A., Kosterev, A. A., Roller, C., Curl, R. F., and Tittel, F. K. (2004) Mid-infrared quantum cascade laser based off-axis integrated cavity output spectroscopy for biogenic nitric oxide detection. *Appl Opt* 43, 2257–2265.
35. Silva, M. L., Sonnenfroh, D. M., Rosen, D. I., Allen, M. G., and O'Keefe, A. (2005) Integrated cavity output spectroscopy measurements of NO levels in breath with a

pulsed room-temperature QCL. *Appl Phys B* 81, 705–710.
36. Bakhirkin, Y. A., Kosterev, A. A., Curl, R. F., Tittel, F. K., Yarekha, D. A., Hvozdara, L., Giovannini, M., and Faist, J. (2006) Sub-ppbv nitric oxide concentration measurements using cw thermoelectrically cooled quantum cascade laser-based integrated cavity output spectroscopy. *Appl Phys B* 82, 149–154.
37. McCurdy, M. R., Bakhirkin, Y. A., and Tittel, F. K. (2006) Quantum cascade laser-based integrated cavity output spectroscopy of exhaled nitric oxide. *Appl Phys B* 85, 445–452.
38. McCurdy, M. R., Bakhirkin, Y., Wysocki, G., and Tittel, F. K. (2007) Performance of an exhaled nitric oxide and carbon dioxide sensor using quantum cascade laser-based integrated cavity output spectroscopy. *J Biomed Optics* 12, R1–R12.
39. Elia, A., Lugarà, P. M., and Giancaspro, C. (2005) Photoacoustic detection of nitric oxide by use of a quantum cascade laser. *Opt Lett* 30, 988–990.
40. Di Franco, C., Elia, A., Spagnolo, V., Scamarcio, G., Lugarà, P. M., Ieva, E., Cioffi, N., Torsi, L., Bruno, G., Losurdo, M. et al. (2009) Optical and electronic NO_x sensors for applications in mechatronics. *Sensors* 9, 3337–3356.
41. Grossel, A., Zéninari, V., Joly, L., Parvitte, B., Durry, G., and Courtois, D. (2007) Photoacoustic detection of nitric oxide with a Helmholtz resonant quantum cascade laser sensor. *Infrared Phys Techn* 51, 95–101.
42. Spagnolo, V., Kosterev, A. A., Dong, L., Lewicki, R., and Tittel, F. K. (2010) NO trace gas sensor based on quartz-enhanced photoacoustic spectroscopy and external cavity quantum cascade laser. *Appl Phys B* 100, 125–130.
43. Ganser, H., Horstjann, M., Suschek, C. V., Hering, P., and Mürtz, M. (2004) Online monitoring of biogenic nitric oxide with a QC laser-based Faraday modulation technique. *Appl Phys B* 78, 513–517.
44. Sabana, H., Fritsch, T., Boyomo Onana, M., Bouba, O., Hering, P., and Mürtz, M. (2009) Simultaneous detection of ^{14}NO and ^{15}NO using Faraday modulation spectroscopy. *Appl Phys B* 96, 535–544.
45. Lewicki, R., Doty, J. H., Curl, R. F., Tittel, F. K., Wysocki, G. (2009) Ultrasensitive detection of nitric oxide at 5.33 μm using external cavity quantum cascade laser based Faraday rotation spectroscopy. Published online before print Jul 22, doi: 10.1073/pnas.0906291106.